ON THE ESTIMATION OF LOCAL SLOPES

J. Schleicher, J. C. Costa, L. T. Santos, A. Novais, and M. Tygel

email: *lucio@ime.unicamp.br*

keywords: *Local slopes, CRS, parameter estimation, traveltime attributes*

ABSTRACT

Current algorithms for the estimation of Common Reflection Surface (CRS) parameters are based on one- or multi-parameter coherency analysis (semblance) schemes applied to the data. Such procedures, besides computationally expensive, leads to significant uncertainties on the searched parameters. Conventional semblance methods can be avoided for a number imaging tasks if local slopes can be directly extracted from prestack data, for example, by filtering schemes. Although the idea is not at all new, recent literature shows its revival for various purposes, such as velocity analysis, tau-p imaging, migration to zero offset and time migration. Here, we discuss several different ways of extracting the desired slope information from the data. We propose a simple, straightforward correction to linear plane-wave destructors. The correction is based on the observation that additionally to the local slope, also its inverse can be extracted from the data in a fully analogous way. Combining the information of both extractions yields a simple but powerful correction to the local slopes. In our numerical examples, the naive application of simple linear plane-wave destructors with our simple, straightforward correction produced results of high quality, even in an example with a rather high noise level and interfering events.

INTRODUCTION

The estimation of kinematic attributes of locally coherent events, in seismic data or seismic images, is an essential step for several recent developments in seismic data processing and velocity model building. Perhaps, the most visible ones are those connected with seismic tomography in which, not only traveltimes but also slowness components of events and possible other time-domain attributes are used for velocity model building. Famous examples are stereo-tomography (Billette and Lambaré, 1998; Billette et al., 2003) and NIP-wave tomography (Duveneck, 2004). Locally coherent events are also applied to velocity-independent time imaging Fomel (2007b).

The estimation of kinematic attributes is usually performed in two steps. The first one is a detection step based on local coherence analysis and the second one is an extraction step based on the coherence level and continuity of the event. This report investigates different implementations of plane-wave destructors for automatic detection of locally coherent events.

Two implementations use small moving windows through data. In the first algorithm, a single slope at the center of the window is computed by linear least squares. The second algorithm implements the prediction-error filter approach proposed by Fomel (2002). We compare these moving-window strategies with a global inversion of the slope field proposed by Fomel (2002). The global slope estimation admits different alternatives of smoothing the slowness field (Fomel, 2007a) by regularization, but is computationally demanding. The slope estimation using local windows is computationally very fast compared to the global estimation alternative and less dependent on prior information.

We present numerical experiments using the local and global strategies for slope estimation on a simple synthetic data, corrupted by white noise. These initial results suggest that the estimation of event slopes using local windows can be a very efficient alternative to the detection of locally coherent events.

PLANE-WAVE DESTRUCTORS

The extraction of local slopes is done by so-called plane-wave destructors. Let us briefly review the underlying theory.

Linear plane-wave destructors

The differential equation for a local plane wave is given by

$$\psi_x(x,t) + p\ \psi_t(x,t) = 0, \quad \psi(0,t) = f(t), \tag{1}$$

where $\psi(x,t)$ is the wavefield, x is the offset, t is time, and p is the local slope (ray parameter or slowness), which may depend on x and even on t, $p = p(x,t)$. In the case that p depends only on x, equation (1) admits the simple solution,

$$\psi(x,t) = f(t - P(x)), \quad P(x) = \int_0^x p(y)\ dy. \tag{2}$$

In particular, if p is constant, we have

$$\psi(x,t) = f(t - p\ x). \tag{3}$$

Our goal is to estimate the local slope $p(x,t)$ for any seismic section which, in general, containing not only plane-wave events but also curved ones.

The first approach is basically the technique presented in Claerbout (2004). For each pair (x_0,t_0) in the seismic section, we select a small window of points x_i, t_j with $(i,j) \in W$ around that point. Let $\psi_x(x_i,t_j)$ and $\psi_t(x_i,t_j)$ be the discretized values for the derivatives ψ_x and ψ_t, respectively, in the selected window. We compute the partial derivatives in the Fourier domain. In order to accomplish with equation (1), we minimize the quadratic residual

$$R(p) = \sum_{(i,j)\in W} \left[\psi_x(x_i,t_j) + p\ \psi_t(x_i,t_j)\right]^2 \tag{4}$$

where W denotes the window. The solution is easily found as

$$\langle p\rangle = \langle p(x_0,t_0)\rangle = -\frac{\sum_{(i,j)\in W} \psi_x(x_i,t_j)\psi_t(x_i,t_j)}{\sum_{(i,j)\in W} \psi_t^2(x_i,t_j)}\ . \tag{5}$$

where (x_0,t_0) is the center of the selected window.

One measure for the fit is given by the normalized correlation,

$$E(x_0,t_0) = 1 - \frac{R(\langle p\rangle)}{R(0)} = \frac{\left[\sum_{(i,j)\in W} \psi_x(x_i,t_j)\psi_t(x_i,t_j)\right]^2}{\left[\sum_{(i,j)\in W} \psi_t^2(x_i,t_j)\right]\left[\sum_{(i,j)\in W} \psi_x^2(x_i,t_j)\right]}. \tag{6}$$

Observe that $0 \le E \le 1$. In fact, E has all the properties of the classical semblance

$$S(x_0,t_0) = \frac{1}{N_x}\frac{\left[\sum_{i\in W_x} \psi\left(x_i, t_0 + \langle p\rangle(x_i - x_0)\right)\right]^2}{\sum_{i\in W_x} \psi^2\left(x_i, t_0 + \langle p\rangle(x_i - x_0)\right)}\ , \tag{7}$$

where N_x is the number of traces in the window W_x in x.

It is to be noted that equation (1) can be equivalently written as

$$q\psi_x(x,t) + \psi_t(x,t) = 0, \tag{8}$$

where $q = 1/p$. This points towards the possibility of extracting q in the very same manner as described above for p. The solution for q, corresponding to equation (5) for p, reads

$$\langle q\rangle = \langle q(x_0,t_0)\rangle = -\frac{\sum_{(i,j)\in W} \psi_x(x_i,t_j)\psi_t(x_i,t_j)}{\sum_{(i,j)\in W} \psi_x^2(x_i,t_j)}\ . \tag{9}$$

Comparing equations (5) and (9), we see that estimation of p or q is equivalent and requires the computation of the same quantities. Those are also the quantities that enter the computation of $E(x_0, t_0)$ in equation (6), which can be easily seen to be nothing more than

$$E(x_0, t_0) = \langle p \rangle \, \langle q \rangle \, . \tag{10}$$

If we suppose that the estimates are proportional to the true value of the corresponding quantity, i.e.,

$$\langle p \rangle = \alpha \, p \qquad \text{and} \qquad \langle q \rangle = \beta \, \frac{1}{p}, \tag{11}$$

then equation (10) becomes

$$E(x_0, t_0) = \alpha\beta \, . \tag{12}$$

Generally, the proportionality factors α and β are due to the noise in the data and thus both smaller than one. Under the further assumption that $\alpha \approx \beta$, we have

$$E(x_0, t_0) \approx \alpha^2 \, , \tag{13}$$

and thus

$$\alpha \approx \sqrt{E} \, . \tag{14}$$

Combining equations (11) and (14), we obtain another estimator for the slope:

$$\langle p \rangle_E = \langle p \rangle / \sqrt{E} = \sqrt{\frac{\langle p \rangle}{\langle q \rangle}} \, . \tag{15}$$

Our numerical experiments indicate that this estimator is more robust than the one of equation (5) in the presence of noise.

Nonlinear plane-wave destructors

We compared the two linear estimators above with the nonlinear plane-wave destructors proposed by Fomel (2002). The nonlinear slope estimation is based on the frequency-domain equation

$$\frac{d\Psi(x, \omega)}{dx} + i\omega p \Psi(x, \omega) = 0 \, . \tag{16}$$

The solution to this equation defines the prediction-error filter

$$P(x + \Delta x, \omega) - e^{i\omega p \Delta x} P(x, \omega) = 0 \, . \tag{17}$$

This solution defines a prediction filter for a neighbouring trace that is nonlinear in the slope p. The numerical implementation is based on rational approximations for the exponential (Fomel, 2007b).

We tested two implementations of nonlinear plane-wave destructor, these being the estimation of p in a local window and the global estimation of p in the whole section. The global estimation requires regularization to produce stable results. We required the solution to have a minimum gradient. Each nonlinear iteration solves the linear system

$$\begin{aligned} \mathbf{F}(\mathbf{p}_0)\delta\mathbf{p}\mathbf{d} + \mathbf{F}(\mathbf{p}_0)\mathbf{d} &= \mathbf{0} \, , \\ \lambda_1 \mathbf{D}_x \delta\mathbf{p} &= \mathbf{0} \, , \\ \lambda_2 \mathbf{D}_t \delta\mathbf{p} &= \mathbf{0} \, , \end{aligned} \tag{18}$$

where $\mathbf{F}(\mathbf{p}_0)$ represents the operator convolved with the data, $\mathbf{d}$; $\mathbf{D}_x$ and $\mathbf{D}_t$ are difference operators and λ_1, λ_2 are the regularization parameters. Moreover, $\delta\mathbf{p}$ represents the correction to the slope field to be estimated, i.e., the correction vector for all individual values of p for all points in the section, and $\mathbf{p}_0$ is the slope field prior to the current iteration.

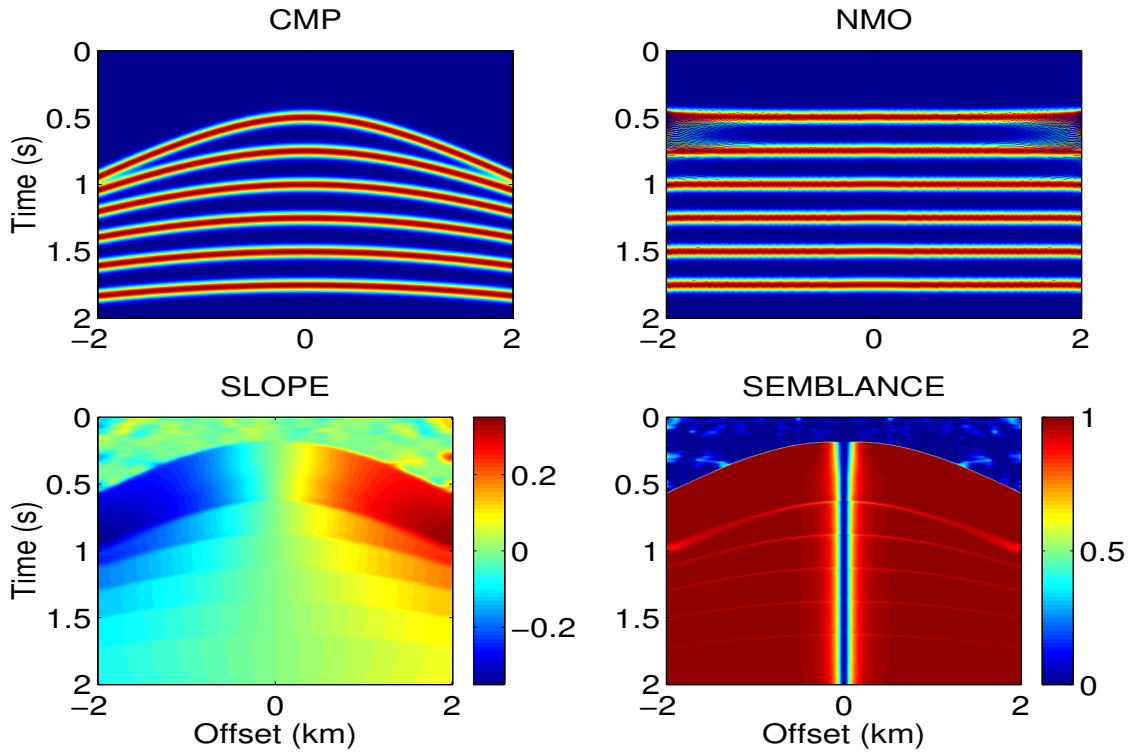

Figure 1: CMP, NMO, Slope and Semblance sections. Noise level = 0%.

SYNTHETIC EXAMPLES

Automatic NMO correction

We tested the indicated technique in two different applications. The first is an automatic NMO correction based on local slopes. To compute the NMO section, we use the fact that the ray parameter for the reflection ray in the CMP gather is given by the traveltime slope (see, e.g., Castagna and Backus, 1993), i.e.,

$$p = \frac{dT}{dx} = \frac{C\ x}{T}, \quad \text{where} \quad T = \sqrt{T_0^2 + C\ x^2}. \tag{19}$$

where T_0 is the zero-offset (ZO) traveltime and C is a parameter. If we know the local slope $p = p(x,t)$ in the CMP gather, we can use equations (19) to eliminate the velocity-dependent parameter C from equation (19). Then, we find the new moveout equation,

$$T_0 = T_0(x,t) = \sqrt{t^2 - C\ x^2} = \sqrt{t^2 - t\ x\ p(x,t)} \tag{20}$$

as a function of the local slope. The procedure that achieves the NMO correction is then to transfer the sample in the CMP section at (x,t) to the NMO section at (x,t_0). This can be done fully automatically.

The results for noise-free data from a simple synthetic model of a horizontally stratified medium are shown in Figure 1. We have plotted the CMP section and the corresponding NMO section using the slopes estimated using equation (5). Figure 2 shows the results for the same model with 30% added noise to the CMP section. For the noisy data, the derivatives of the wavefield have been smoothed by a two-dimensional moving average with a window of $N_t = 10$ and $N_x = 5$. Both results are satisfactory, demonstrating that the estimation of local slopes is sufficiently stable to permit an automatic NMO correction even for noisy data.

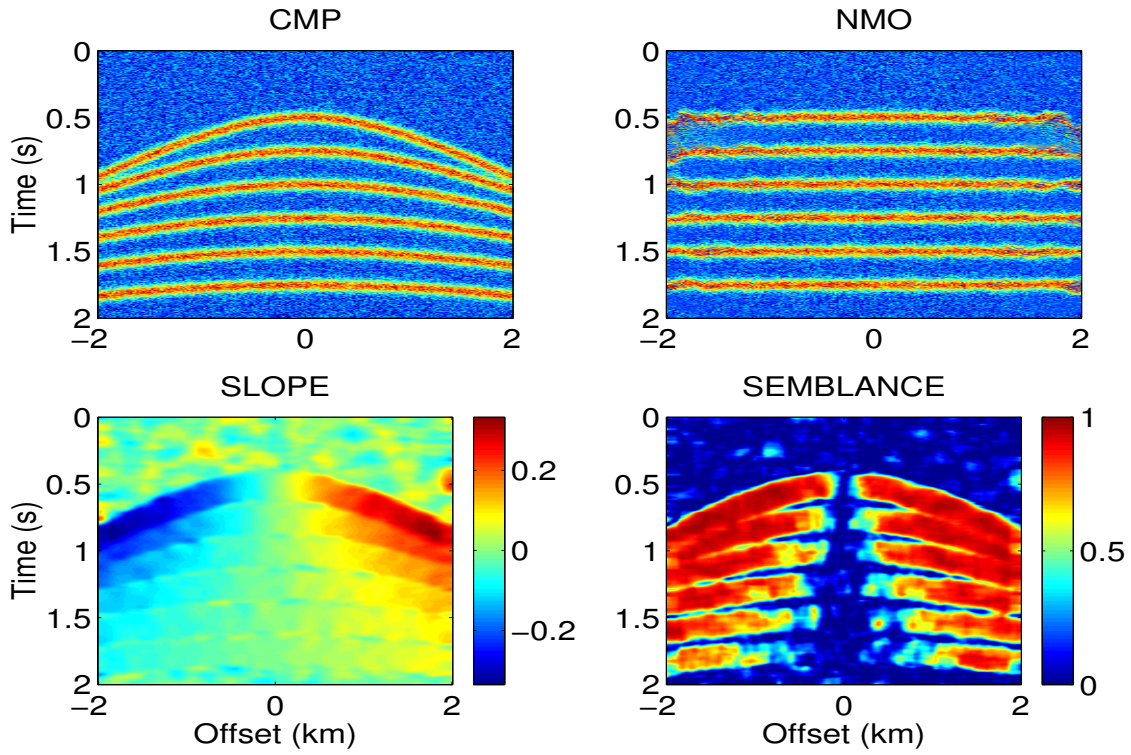

Figure 2: CMP, NMO, Slope and Semblance sections. Noise level = 30%.

Extraction of local slopes

In the second example, we tested the extraction of the local slopes as an event attribute. This type of application has its meaning in the context of stereotomography or the CRS stack, where event dips are crucial parameters.

For our tests we devised a model with a single trough-shaped reflector separating two homogeneous interfaces (see Figure 3). We modeled synthetic data with the Kirchhoff integral and added white noise at a level of 20% of the maximum amplitude. For the subsequent slope extraction, we then applied an AGC. Note the distorted bow-tie structure in the data. This was chosen to make it a little harder to extract correct slopes.

Next we applied the above slope extraction techniques to these data. The resulting semblance and slope sections are shown in Figures 4 and 5, respectively. Also shown in these figures are the paths of maximum semblance along which the slopes are extracted from these panels. As before, the derivatives of the wavefield were smoothed with a two-dimensional moving average with a window of $N_t = 10$ and $N_x = 5$.

For the extraction of the slopes, one possible measure of reliability is the semblance section. However, establishing a semblance threshold above which all values are considered reliable and below which all values are discarded tuns out not to be a very successful strategy. If we choose the threshold to be a semblance value of 0.75, we obtain the picture in Figure 6. We recognize that while some regions of the events are well represented, there are large parts of the events where no slope will be extracted. Unfortunately, this cannot be remedied by decreasing the threshold, which mainly leads to the extraction of more and more incorrect slope values.

The quality of the extracted slope values can be evaluated in Figure 7. Except for the nonlinear plane-wave destructors in the whole section, practically all extracted slope values correspond nicely to the true values along the three events. However, as expected from Figure 6, there are quite considerable gaps where no slope values have been extracted.

There is another way of extracting slopes. This is already indicated in Figures 4 and 5. It consists of

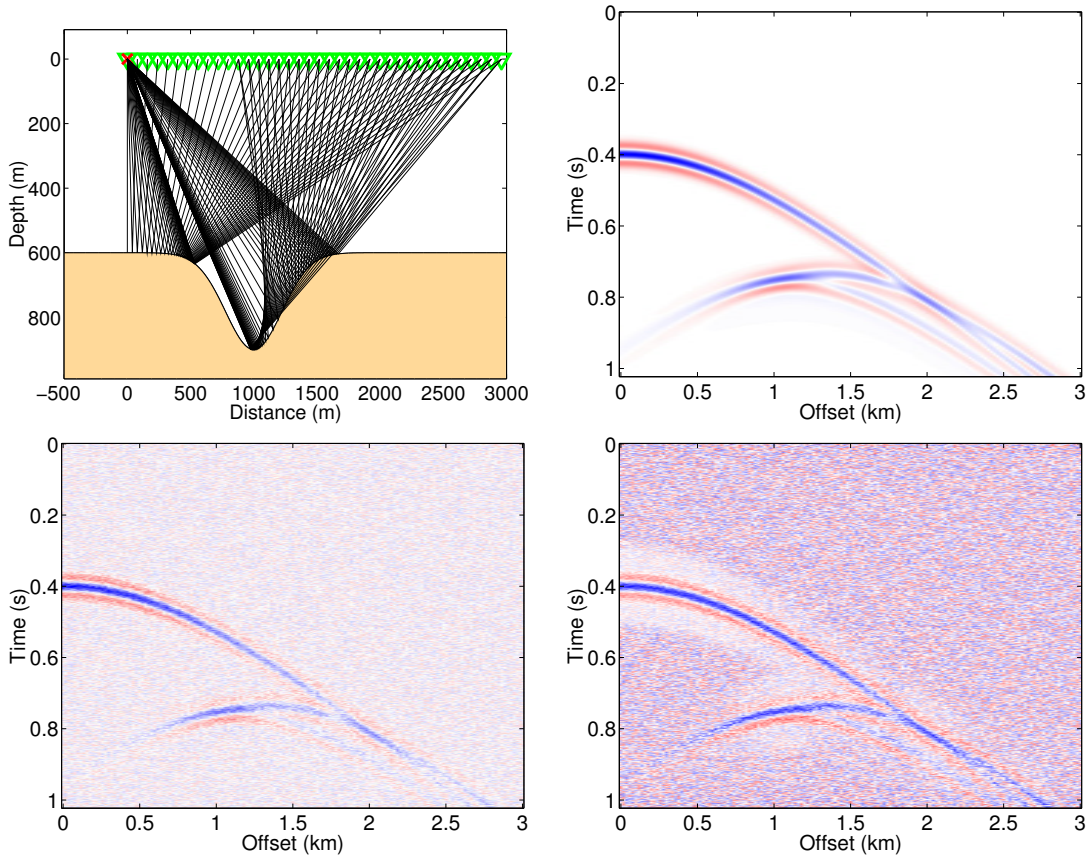

Figure 3: Model and data for the slope extraction. Top left: Model and ray family. Top right: Kirchhoff data. Bottom left: Kirchhoff data with 20% random noise. Bottom right: Noisy data after AGC.

extracting the slope values along the maximum-semblance curve, independently of the absolute semblance at the location. The results of this procedure are shown in Figure 8. We observe high-quality slope values along the first part of the event. The quality of the extracted slopes drops only where the events interfere, thus altering the true slope values. In this region, the windowed nonlinear plane-wave destructors seem to do the best job. However, the simple and fast corrected estimate of equation (15), when guided by any of the chosen semblance functions, also provides very good slope estimates. The whole-section nonlinear plane-wave destructors suffer more from the interfering events.

The consequence of eliminating slope values with semblance below a threshold can be understood with the help of Figure 9. We see that even though large parts of perfectly well estimated slope values have already been discarded, still some of the bad estimates pass the criterion. The windowed nonlinear plane-wave destructors suffers the least, since its semblance exceeds the threshold almost everywhere. Still in this case, the eliminated slopes are better estimates than some of the retained ones. This is another indication that simple semblance masking is not the best way to proceed in order to extract reliable slope values from the data.

It is to be remarked that the results of the whole-section nonlinear plane-wave destructors depend on the regularization parameters for the damping of the roughening operator in the optimization. To understand this dependence, Figure 10 shows the extracted slopes along the first arrival as a function of the regularization parameter. We see that stronger damping leads to more stable slope values. On the other hand, the estimated values become lower and lower, thus more and more underestimating the true slopes. Note that in addition to the effects on the extracted slopes, stronger damping leads to faster convergence and higher semblance values.

CONCLUSIONS

In this paper, we have shown how local slopes can be extracted from a seismic section. Local slopes are important attributes for a number of different tasks, ranging from velocity analysis to an automatic NMO correction, CRS stack, and stereotomography.

We have discussed several different ways of extracting the desired slope information from the data. We have proposed a simple, straightforward correction to the linear plane-wave destructors of Claerbout (2004). The correction is based on the observation that additionally to the local slope, also its inverse can be extracted from the data in a fully analogous way. Combining the information of both extractions yields a simple but powerful correction to the local slopes.

In our numerical examples, the naive application of simple linear plane-wave destructors with our simple, straightforward correction produced results of high quality, even in an example with a rather high noise level and interfering events. Only a windowed application of nonlinear plane-wave destructors produced slightly better results. The application of nonlinear plane-wave destructors in the whole section at once under regularization with a roughening operator as proposed by Fomel (2002) turned out to be strongly dependent on the chosen regularization parameters. Moreover, in the region of interfering events, the extracted slope values where of lower quality.

ACKNOWLEDGMENTS

This work was kindly supported by the *National Council of Scientific and Technological Development (CNPq)*, Brazil, and the sponsors of the *Wave Inversion Technology (WIT) Consortium*, Germany.

REFERENCES

Billette, F. and Lambaré, G. (1998). Velocity macro-model estimation from seismic reflection data by stereotomography. *Geophys. J. Int.*, 135(2):671–690.

Billette, F., Le Bégat, S., Podvin, P., and Lambaré, G. (2003). Practical aspects and applications of 2D stereotomography. *Geophysics*, 68(3):1008–1021.

Castagna, J. P. and Backus, M. M. (1993). *Offset-Dependent Reflectivity – Theory and Practice of AVO Analysis*. SEG.

Claerbout, J. F. (2004). *Earth Sounding Analysis: Processing versus Inversion*. Blackwell Scientific Publications.

Duveneck, E. (2004). 3D tomographic velocity model estimation with kinematic wavefield attributes. *Geophysical Prospecting*, 52:535–545.

Fomel, S. (2002). Applications of plane-wave destruction filters. *Geophysics*, 67:1946–1960.

Fomel, S. (2007a). Shaping regularization in geophysical-estimation problems. *Geophysics*, 72:R29–R36.

Fomel, S. (2007b). Velocity-independent time-domain seismic imaging using local event slopes. *Geophysics*, 72:S139–S147.

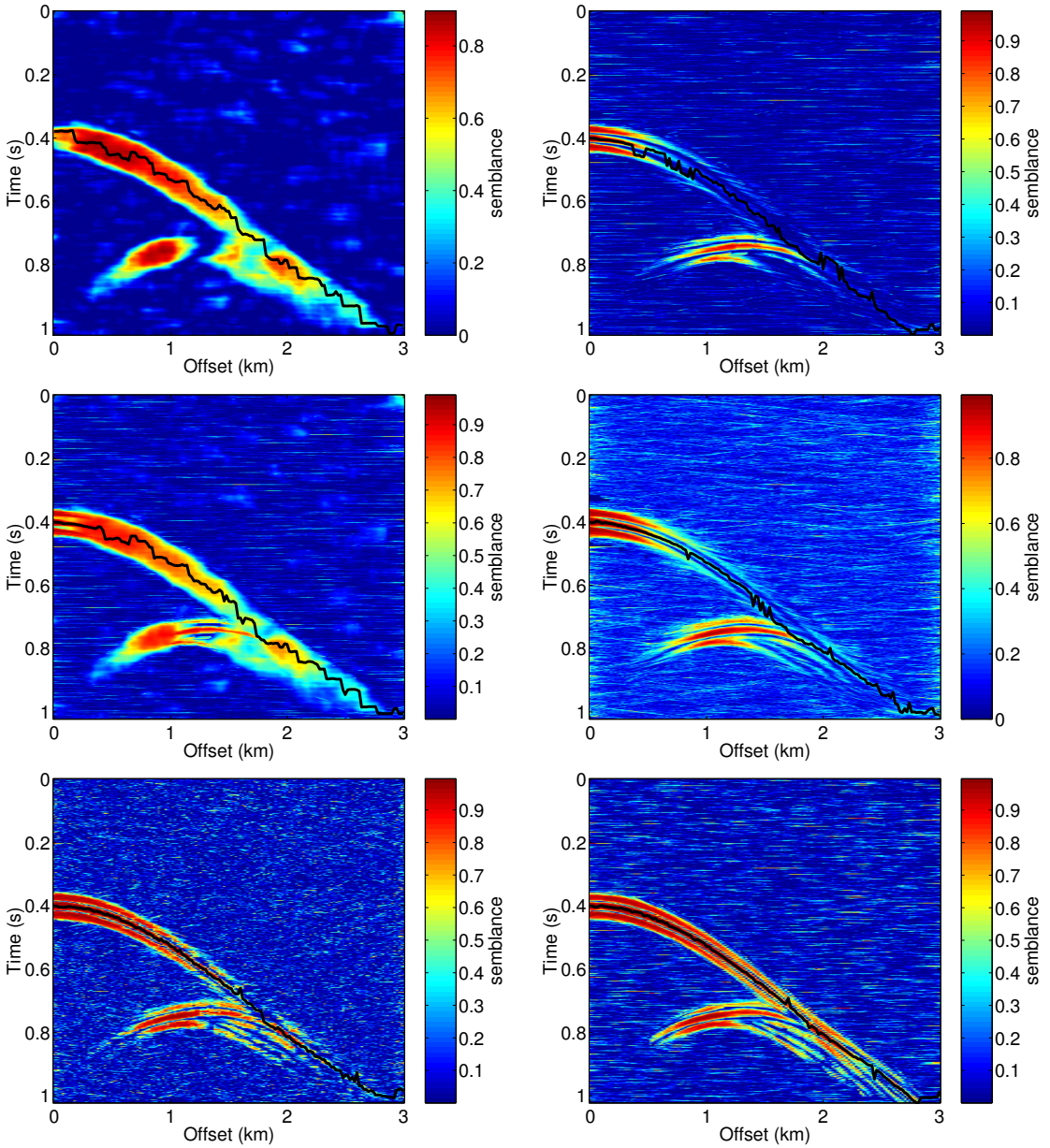

Figure 4: Final semblance sections and curves of maximum semblance along the first arrival. Top left: Calculated using equation (6). Top right: Calculated using equation (7) along short lines with the extracted slope at every point. Center left: Maximum semblance of the two above. Center right: Optimization of the classical semblance [equation (7)] using the previous p as initial value. Bottom left: Calculated using the nonlinear plane-wave destructors of Fomel (2002) in the whole section. Bottom right: Calculated using the nonlinear plane-wave destructors of Fomel (2002) in 10×3 windows.

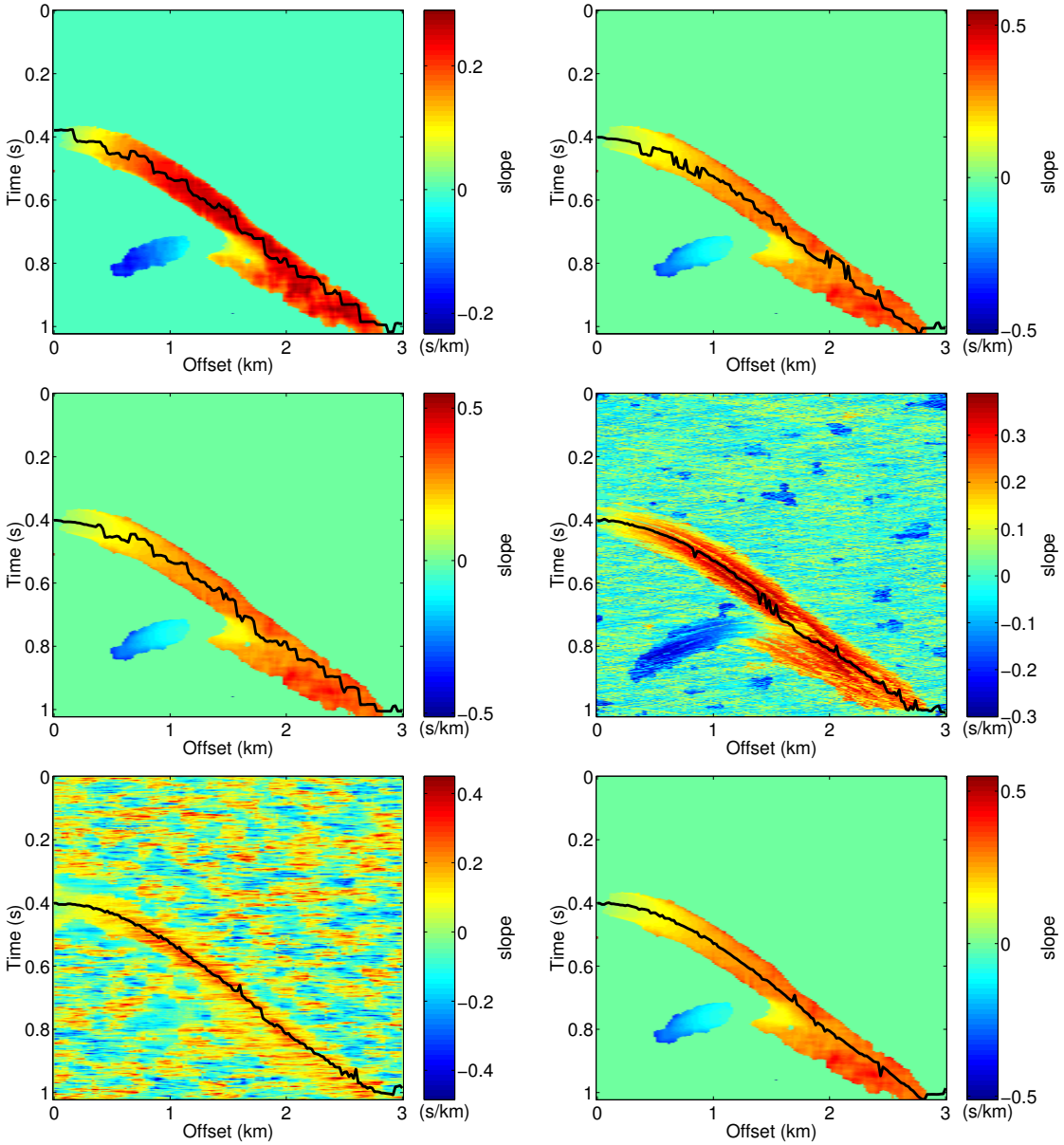

Figure 5: Slope panels with overlain maximum-semblance curves. Top left: Calculated using equation (5). Top right: Calculated using equation (15) in 10×5 windows. Center left: Calculated using equation (15) in 10×5 windows. Center right: Calculated using an optimization of the classical semblance [equation (7)] using the previous p as initial value. Bottom left: Calculated using the nonlinear plane-wave destructors of Fomel (2002) in the whole section. Bottom right: Calculated using the nonlinear plane-wave destructors of Fomel (2002) in 10×3 windows.

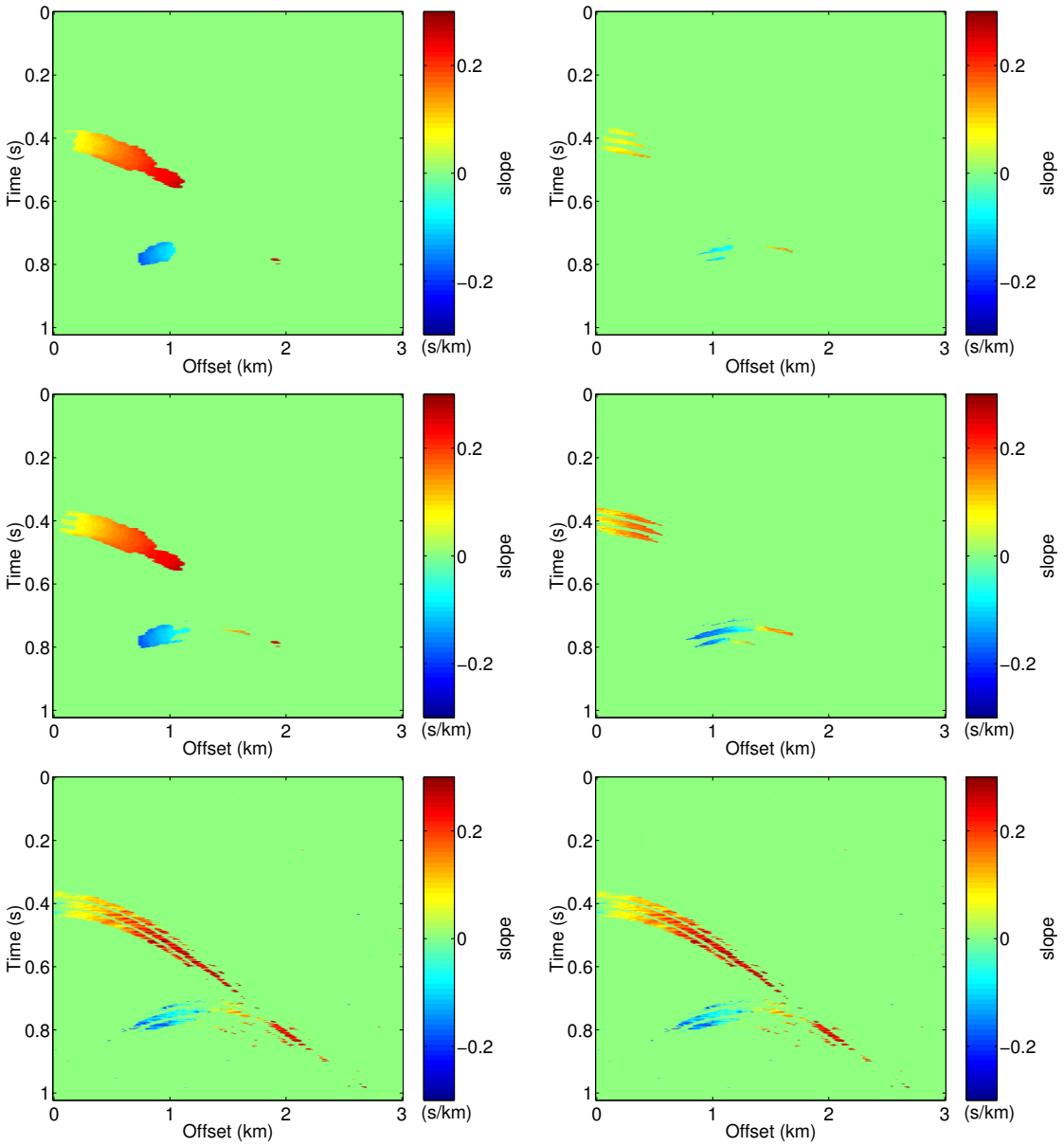

Figure 6: Slope extraction by semblance threshold. Shown are all values of slopes at points where the semblance exceeds 0.75. Top left: Semblance from equation (6). Top right: Semblance from equation (7) along short lines with the extracted slope at every point. Center left: Maximum semblance of the two above. Center right: Optimized semblance. Bottom left: Semblance from nonlinear plane-wave destructors in the whole section. Bottom right: Semblance from windowed nonlinear plane-wave destructors.

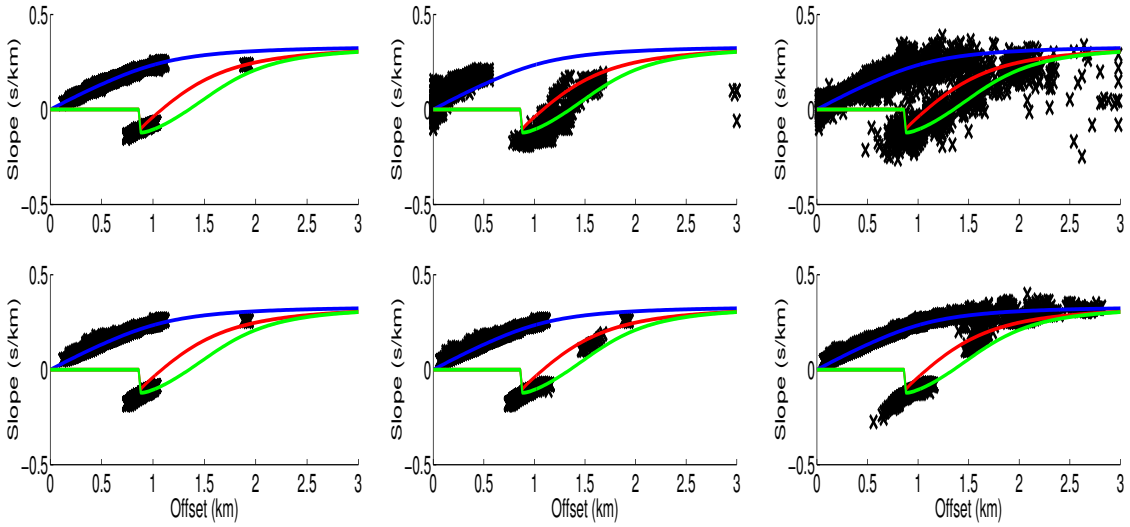

Figure 7: Slope extraction by semblance threshold. Shown are all values of slopes at points where the semblance exceeds 0.75 as a function of their horizontal position. Also indicated are the true slopes of the three events as determined by ray theory. Left: Accepted slopes as calculated with equation (5) (top) and equation (15) (bottom). Center: Accepted slopes with classical semblance equation (5) (top) and semblance maximum (bottom). Right: Accepted slopes from nonlinear plane-wave destructors in the whole section (top) and in windows (bottom).

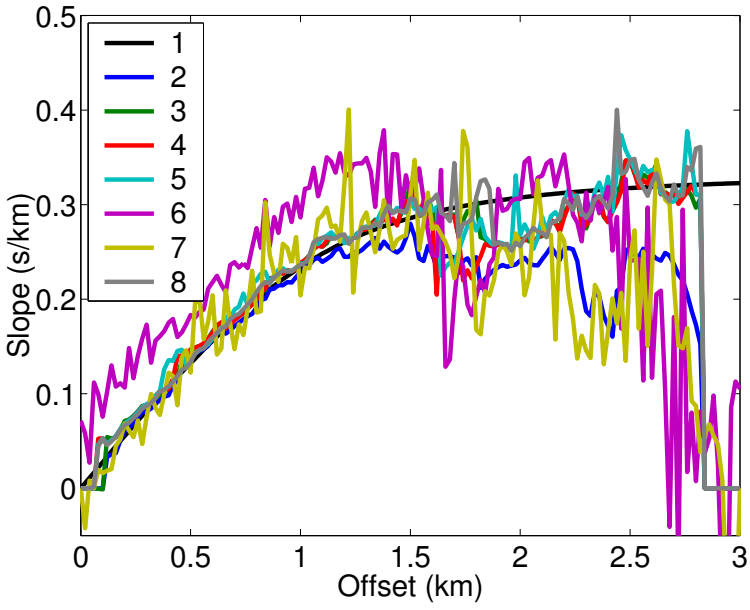

Figure 8: Slope values extracted along the maximum-semblance curve of the first arrival. 1: True slope along the first arrival. 2. Calculated with formula (5), semblance of equation (6). 3: Calculated with formula (15), semblance of equation (6). 4: Calculated with formula (15), classical semblance. 5: Calculated with formula (15), maximum of last two semblances. 6: Optimized slope, optimized classical semblance. 7. Nonlinear plane-wave destructors in whole section. 8. Windowed nonlinear plane-wave destructors.

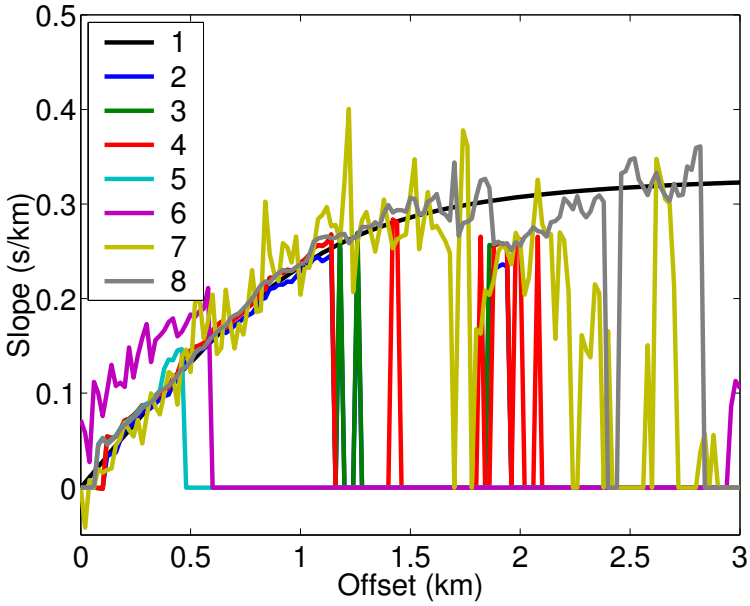

Figure 9: Slope values extracted along the maximum-semblance curve of the first arrival with semblance above the threshold of 0.75. 1: True slope along the first arrival. 2. Calculated with formula (5), semblance of equation (6). 3: Calculated with formula (15), semblance of equation (6). 4: Calculated with formula (15), classical semblance. 5: Calculated with formula (15), maximum of last two semblances. 6: Optimized slope, optimized classical semblance. 7. Nonlinear plane-wave destructors in whole section. 8. Windowed nonlinear plane-wave destructors.

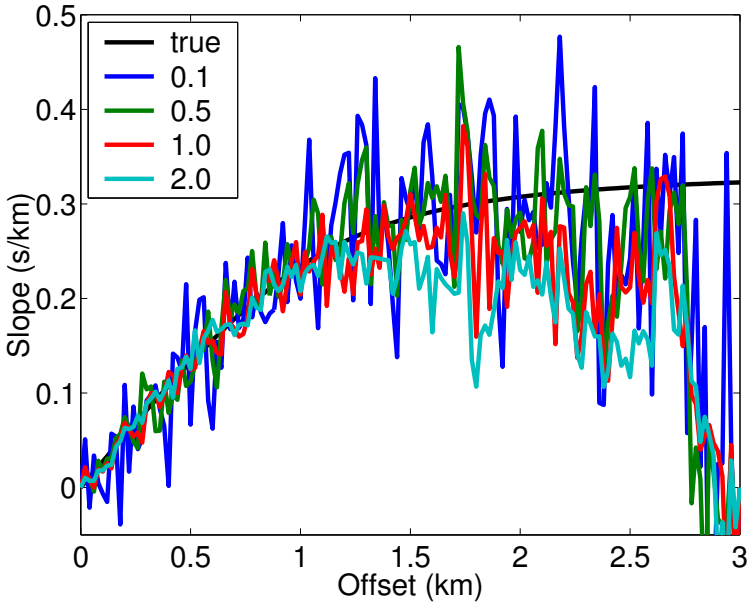

Figure 10: Extracted slope values of whole-section nonlinear plane-wave destructors with different regularization parameters for the damping of the roughening operator.